A Study on the Apparent Friction Angle Mobilized during the Undrained Loading in Long Run-out Landslides

AUTHOR(S):

LEE, Jong-hak; SASSA, Kyoji

Bull. Disas. Prev. Res. Inst., Kyoto Univ., Vol. 45, Part 4, No. 393, March, 1996

A Study on the Apparent Friction Angle Mobilized during the Undrained Loading in Long Run-out Landslides

By Jong-hak LEE and Kyoji SASSA

(Manuscript received on July 19, 1995, revised on Mar. 12, 1996)

Abstract

Long run-out landslides have often caused catastrophic disasters throught the world. These landslides have low apparent friction angles during motion in comparison with the usual values of internal friction angle of soils and rocks. Using the ring shear apparatus, this paper experimentally investigated the behavior and the mechanism of shear resistance mobilized during rapid loading on soil layers, which is very likely to occur in long run-out landslides.

After residual state was obtained by constant speed shearing at a low normal stress in dry soils, normal stress was rapidly increased while shearing speed was maintained. In some cases, the stress deviated from the failure line, and the shear state was changed from the plastic failure state to the pre-failure deformation state even though shear deformation was continued. It was found out that the ratio of the shear speed to the loading speed should be greater than a critical value for the plastic failure state to be maintained throughout rapid loading.

The ring shear apparatus was improved so that the undrained loading tests could be implemented and the generated pore pressure could also be measured. The undrained loading ring shear tests for the saturated samples taken from the alluvial deposits of the 1983 Sale landslide in China, as well as for the torrent deposits of the 1984 Ontake debris avalanche, Japan were conducted. These tests produced a high excess pore water pressure during the undrained loading and reproduced low apparent friction angles mobilized in both long run-out landslides.

In the undrained ring shear tests of the torrent deposits from the Ontake debris avalanche, a high excess pore water pressure was generated not only by normal stress loading, but also only by shearing keeping normal stress constant. It was estimated that those coarse and volcanic grains were crushed during shearing and it caused negative dilatancy to generate excess pore pressure. On the contrary, the sample from the alluvial deposits from the Sale landslide did not show the pore water pressure generation due to shearing probably because the long-transported fine silty grains were hardly crushed.

1. Introduction

Scheidegger (1973) visualized an empirical relationship between the distance travelled by a landslide and its volume whereby landslides travel further, the larger their volume. He plotted the ratio of the total vertical height (H) of the traveling path of the landslide to the horizontal travel distance (L) against the volume of landslides, as shown in **Fig. 1**. He called the ratio H/L as the "average coefficient of friction f". This ratio generally decreases as the volume of material increases, especially beyond 10^5 m^3. This higher mobility in larger landslides has been studied by many authors.

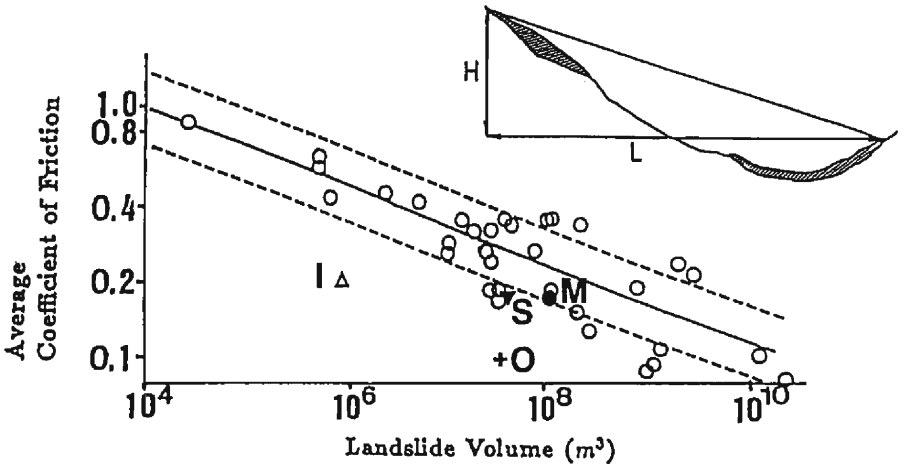

Fig. 1. Correlation between landslide volume (V) and the average coefficient of friction which is total height (H) divided by total travel distance (L) (Scheidegger, 1973). M: Mayu-yama landslide, S: Sale landslide, I: Ichinomiya landslide, O:Ontake debris avalanche

1. 1. Previous studies on high mobility

(1) Flow behavior of granular materials and mechanical fluidization

Hsü (1975), McSaveney (1978), Davies (1982) and Körner (1980, 1982) applied the idea to explain the mobility of debris flows proposed by Bagnold (1954) to the high mobility of large landslides. The concept by Bagnold is that the mechanical state of shearing in granular materials changes from the sliding of grains to collisions of grains at very high strain rate (shear speed), at which the shear resistance becomes smaller.

(2) Air cushion and vaporization of pore fluid

Shreve (1966, 1968) proposed the air-lubrication hypothesis to account for the unusually long run-out motion from his studies of the Blackhawk landslide in California. He speculated that the abnormally small coefficient of friction is due to trapped air; the larger the fallen mass, the more air was trapped to lubricate the sliding mass. Gogule (1978) postulated the role of high-pressure steam generated by frictional heat at the sliding surface in reducing sliding friction by partly supporting the overburden pressure.

(3) Acoustic fluidization and basal pressure waves

Melosh (1979) proposed that the low apparent friction was due to 'acoustic fluidization' induced by a transient strong acoustic wave field. This hypothesis described a high-frequency vibration which may be capable of momentarily relieving the static overburden pressure in limited regions of the landslide mass, allowing sliding to occur in the unloaded regions. Kobayashi (1994) proposed that basal waves are generated in a high velocity motion, and the waves cause mechanical fluidization to decrease the shear

resistance of landslides.

(4) Excess pore pressure generated at the initial failure

Hutchinson (1986) proposed a sliding-consolidation model for flow slides. At the commencement of landslides, a high excess pore pressure is often generated in saturated loose and cohesionless materials. In this case the landslide mass accelerates downslope due to this high pore pressure. During this process, the excess pore pressure is successively dissipated according to consolidation, and the mass will stop after a relatively long travel distance.

1. 2. Undrained loading by the moving landslide mass onto a saturated soil layer

In the case of large-scale landslides, e.g., the Sale landslide in China (Sassa *et al.*, 1992) and the Frank slide in Canada (Cruden and Hungr, 1986), the landslide mass usually reaches the alluvial deposit where the ground water surface is usually connected to a river or lake or sea at a relatively shallow depth. Sometimes, as in the Ontake landslide, large landslide masses move onto the torrent deposits, which are usually saturated at a certain depth. In such cases, undrained loading is not exceptionable, but very probable.

Fig. 2 illustrates the apparent friction angle mobilized during the rapid loading

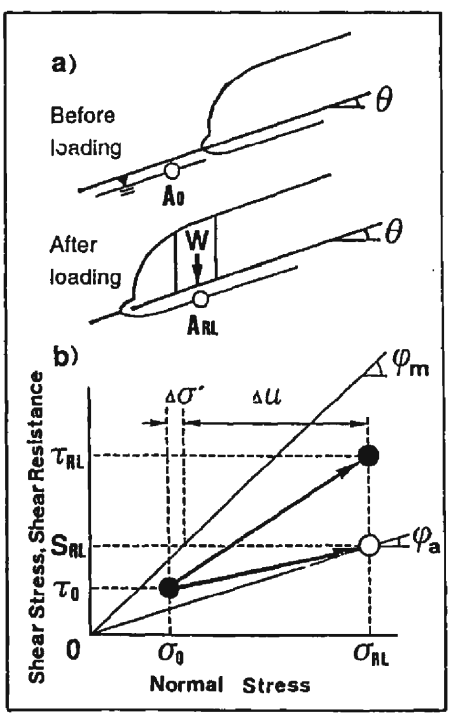

Fig. 2. Stress and shear resistance before/after rapid loading.

situation associated with the motion of landslides. When a landslide mass moves on a saturated soil layer as shown in **Fig. 2-a**), excess pore pressure can be generated in the underlying soil layer if it is saturated. If the location of saturated soil layer is not so deep, a sliding surface can develop on the surface of the saturated layer. This can cause the landslide mass to scrape the soil mass above the sliding surface as it moves. In such situations, the friction angle mobilized along the sliding surface can be small because of the high pore pressure generated by rapid loading.

Fig. 2-b) shows the shear stress and shear resistance mobilized at a point in the saturated soil layer before (A_0) and after rapid loading (A_{RL}). Normal stress and shear stress before loading are equal to (σ_0, τ_0). After rapid loading, shear resistance will correspond to the sum of initial normal stress (σ_0) and an effective normal stress increment ($\Delta\sigma'$), namely S_{RL}. The friction angle mobilized on rapid loading is equal to the gradient of the line connecting the origin to (σ_{RL}, S_{RL}). The angle of this line is called as the apparent friction angle (ϕ_a), and it may be much smaller than the real friction angle during motion (ϕ_m). When the shear resistance after rapid loading (S_{RL}) is lower than the shear stress (τ_{RL}) due to the self-weight of landslide mass after rapid loading as in **Fig. 2-b**), the landslide mass is accelerated. On the contrary, if τ_{RL} is smaller than S_{RL}, the landslide mass is decelerated, but it can still travel longer because of the lower value of the apparent friction, i.e., a lower rate of energy consumption.

Sassa and others postulated the generation of high pore pressure in a saturated soil layer under the ground on which the landslide mass travels, because of undrained loading by the landslide mass. A series of their studies are the base of this paper.

Sassa (1988a) classified three types of pore pressure generation/dissipation along the sliding surface during the motion of landslides, and proposed that Type B is the mechanism of long run-out landslide. He estimated the amount of the excess pore pressure due to the undrained loading indirectly by means of the constant-volume direct shear tests and triaxial tests.

In 1989, Sassa *et al.* (1989) developed a high-speed high-stress ring shear apparatus for the study of long run-out landslides, that was capable of reproducing rapid loading conditions (namely associated with three types of landslides) in the apparatus. Using this apparatus, Sassa *et al.* (1989)simulated the situation of rapid loading by the moving landslide mass, and found that the stress path deviated from the failure line during rapid loading, namely the apparent friction angle became small.

Fukuoka *et al.* (1989) and Fukuoka (1991) studied the internal friction angle of dry soils during a long travel distance up to 100 m and at various shear speeds. He confirmed that the internal friction angle during motion remained at almost the same values, though a few degrees change.

Sassa (1992) gave a quantitative interpretation to the empirical relationship between the average coefficient of friction and the landslide volume (**Fig. 1**), using the results of rapid loading ring shear tests of the alluvial deposit taken from the Sale landslide.

Sassa and Lee (1993) gave a quantitative explanation to the long travel distances of the Sale landslide by the measurement of friction angle during motion for the sample

taken from the source area of the landslide and by the rapid loading ring shear test on the sample taken from the alluvial deposits of the landslide.

The authors believe that this undrained loading theory represents the most probable mechanism for long run-out landslides among the various mobility theories. However, previous research on undrained theory from Sassa (1988) to Sassa and Lee (1993) did not succeed in to measure the generation of pore pressure during rapid loading. Their papers assumed that the deviation of stress path from the failure line during rapid loading must be the result of generation of pore pressure. And their papers did not examine the shear resistance during rapid loading for dry soils. Therefore, one could not eliminate the possibility that the deviation from the failure line during rapid loading can be caused by other reasons than pore pressure generation. Accordingly, it can be said that the mechanism of shear resistance mobilized during rapid loading has not yet been resolved, and the excess pore pressure generation due to rapid loading has not yet been confirmed experimentally by any measurement. Hence, the aims of this study are as follows;

(1) To investigate the mechanism of shear resistance during rapid loading in dry soils, i.e. under the condition of no pore pressure generation.
(2) To experimentally confirm the generation of pore pressure during undrained loading associated with the motion of landslides, which was assumed by previous studies, but not yet measured, employing an improved high-speed high-stress ring shear apparatus that is capable of the undrained loading test as well as direct measurement of generated excess pore pressure through large shear displacement.
(3) To investigate the mechanism of pore pressure generation during undrained loading, based on the real measurement of generated excess pore pressure for different types of soils.

2. Test Apparatus and Samples

2. 1. General structure of the high-speed high-stress ring shear apparatus

Sassa (1989) has developed a high-speed high-stress ring shear apparatus, which employed in this study.

The sample box consists of an inner and an outer ring. The outer parts of the sample box are made of transparent acrylic resin, allowing observation to be made during testing. The transparent acrylic resin is held in place by a metal frame. The sample box consists of two halves, an upper and a lower part. The lower half is rotated by a servo-control motor, while the upper half is retained to a pillar through the shear load cell. The outer diameter of sample in the shear box is 33 cm and the inner diameter is 21 cm, therefore the shear area of sample is 508.9 cm^2. The sample box is circular and 6 cm wide and 6-8 cm high. The loading plate can be moved vertically to accommodate volume changes during consolidation and shearing.

Six porous metal plates are fixed to the loading plate and the base of the sample box to dissipate the generated pore pressure in the sample box. Vertical needles are fixed to the base of the sample box and the loading plate to prevent slippage of the sample inside

the sample box during shear. In the rapid loading test, normal stress is applied by the loading plate during the process of shear rotation.

Rubber edges are pasted to the upper part of the outer and inner ring. Pressing on the edge of lower part of outer and inner ring, they prevent the leakage of sample during tests. The gap distance between the upper and lower half of the sample box can be kept constant automatically by the servo-control motor by a signal from the gap measuring sensor, with a precision in the order of 0.002 mm. The maximum normal stress which can be applied is 3.8 kgf/cm^2. Shear speed can be varied between 0.001 cm/sec and 150 cm/sec, using four different gears in the gear box.

2. 2. Undrained shear box

The shear box in the high-speed high-stress ring shear apparatus was modified for undrained loading tests, and the pore pressure measurement system was improved to make it possible to measure the generated pore pressure during a large shear displacement, which was accomplished by the great efforts of the members of the Landslide Section of the Disaster Prevention Research Institute, Kyoto University [(Sassa, 1994), (Shoaei and Sassa, 1994)].

A schematic diagram of the modified shear box is shown in **Fig. 3**. On the inside the outer ring and at the height of 2 mm above the shear plane, a gutter of 4 × 4 mm was built around the whole circumference of the outer ring, and two metal filters and one felt cloth filter were placed inside the gutter. On the back of the filters, a gutter of 1 × 1 mm was built to transfer the pore pressure smoothly to the pressure transducer. A hole was punched from the outside of the ring to the gutter. A pore pressure transducer was connected to the hole to measure the pore pressure directly. In the modified shear box, drained/undrained conditions can be controlled freely by switching the valve connected

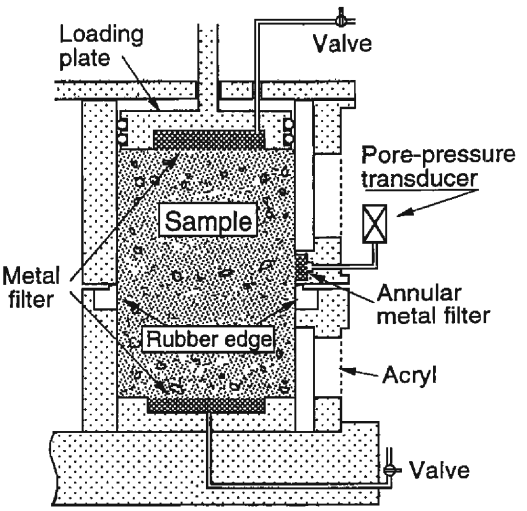

Fig. 3. Schematic disgram of the undrained sample box.

to the loading plate and the bottom of the shear box.

Using this modified ring shear apparatus, undrained loading ring shear tests were carried out for the saturated samples from the alluvial deposits of the Sale landslide, the Lishan landslide, and the torrent deposits of the Ontake debris avalanche.

2. 3. Samples

The following three samples were used, and the grain size distribution of these samples are shown in **Fig. 4.**

(1) Sample from Kyoto University campus: This sample was collected on the Kyoto University campus from alluvial deposits. The sample comprised granitic sandy soils. It was easy to obtain a large volume of samples repeatedly.

(2) Sample from the Sale landslide in China: This sample was taken from the alluvial deposits of the Sale landslide in 1983, China. The sample comprised silty soils, mainly composed of fine grains. The permeability is as low as 2.9×10^{-6} cm/sec.

(3) Sample from the torrent deposits of the Ontake debris avalanche in Japan: This sample was collected from the Denjo river along which the Ontake debris avalanche traveled over 10 km in 1984.

3. Rapid Loading Ring Shear Tests on Dry Samples

To examine the behavior and the mechanism of shear resistance associated with rapid loading of normal stress during a constant speed shearing, rapid loading ring shear tests were carried out on dry soils.

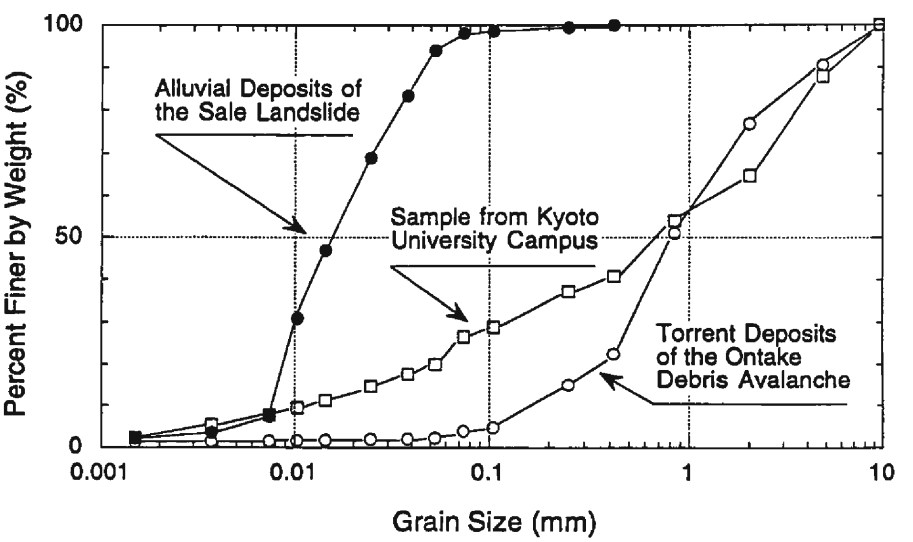

Fig. 4. Grain size distribution of soil samples.

3. 1. Test procedure and test results

Fig. 5 presents the results of two rapid loading tests (Test A and Test B) using dry soils from the Kyoto University campus. The method for the rapid loading tests is shown schematically. The sample is consolidated at the normal stress of 0.5 kgf/cm^2, and the shear strength at residual state (S_1) is measured by shearing at a constant shear speed. The state of sample in this stage is in the plastic failure state, where the stress lies on the failure line and shear displacement continues to proceed under a constant shear stress. Then, normal stress is rapidly increased up to 3.5 kgf/cm^2, while shearing is continued at a constant speed. After normal stress reaches 3.5 kgf/cm^2, normal stress is kept constant and a constant speed shearing is continued to measure the changes in shear stress.

The normal stress was increased from 0.5 kgf/cm^2 to 3.5 kgf/cm^2, it took 8 seconds (Test A) and 7 seconds (Test B), respectively. Loading speed of normal stress was almost equal in both tests, but the shear speed was different, 1.2 cm/sec in Test A and 0.01 cm/sec in Test B, respectively. The stress path of Test A is represented by S_1—S_3. On the contrary, the stress path of Test B was S_1—S_2—S_3. The two stress paths are respectively quite different depending on shear speed. The stress path of Test B apparently deviated from the failure line, while the stress path of Test A probably moved along the failure line. Although these two tests were conducted for dry soils, so that no

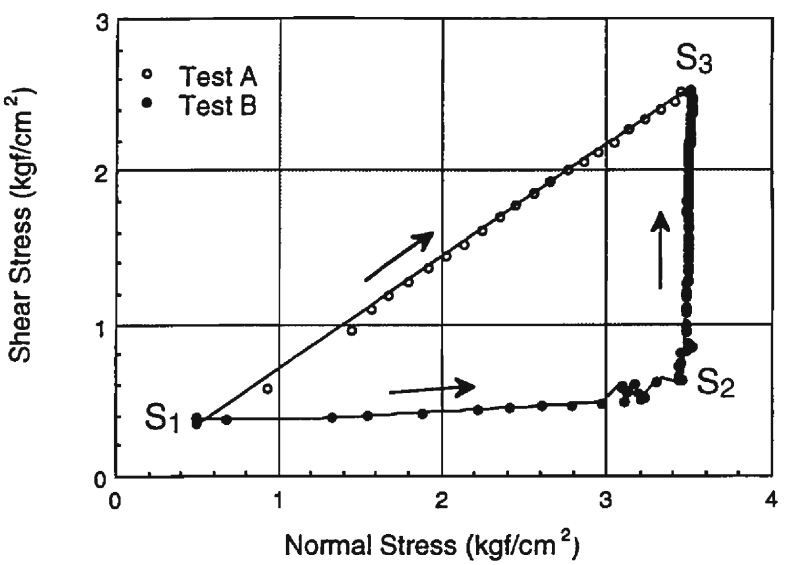

Fig. 5. Test results of the rapid loading ring shear tests on dry sample from Kyoto University campus at two different shearing speeds.
Test A (S1→S3): Shear speed=1.2 cm/sec
Loading time (S1→S3)=8 seconds
Test B (S1→S2→S3): Shear speed=0.01 cm/sec
Loading time (S1→S3)=7 seconds

pore pressure could be generated, the stress path in Test B behaved as if pore pressure were generated. What happened, and how can the stress path of Test B be interpreted ?

3. 2. Interpretation of the test

Let the rapid loading process be shown as the dashed line (A_0 to B) in **Fig. 6**. This continuous process can be assumed as a sum of infinitesimal steps like (A_0 to A_1) during a infinitesimal time step of Δt. We will consider the variation of shear stress and the stress path during the time step of Δt.

The possible change of shear stress is shown in **Fig. 7-a**) and the possible change of stress path is shown in **Fig. 7-b**). The normal stress increment is assumed to take place instantly in **Fig. 6**. Shear stress remains the same at no increment of shear displacement at a moment. Therefore, the stress path should move horizontally as shown in **Fig. 7-b**). As time elapses, shear displacement proceeds, and shear stress increases. The process will be expressed as a curve from A_0 to A_1 in **Fig. 7-a**) and as a line from P_1 to A_1 in **Fig. 7-b**), when the shear displacement is enough for the stress path to reach the failure line, in another expression, for the soils to return to the plastic failure state.

If the shear displacement after loading of normal stress increment is not enough for the stress path to reach the failure line, the change of shear stress and the stress path will be something like lines shown in **Fig. 7-c**) and **Fig. 7-d**), respectively. Before the stress path comes back to the failure line, the next step of normal stress loading is given. In this case, the resulting stress path should deviate from the failure line as shown in **Fig. 7-d**).

In Test A of **Fig. 5**, it is assumed that the state of sample during rapid loading is always in the plastic failure state. Test B of **Fig. 5** is the case in which the state of soils during rapid loading is out of the plastic failure state, but changes to that of pre-failure deformation in which the shear stress is smaller than the shear strength. Therefore, the stress path of Test B from S_2 to S_3 in **Fig. 5** is not the process of pore pressure dissipa-

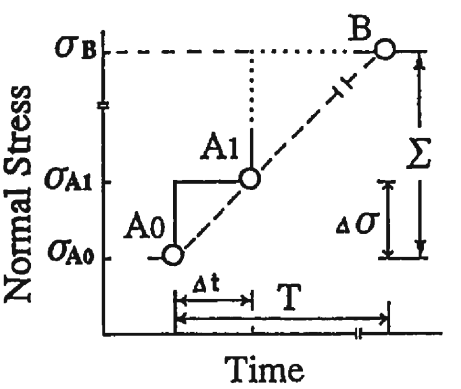

Fig. 6. Imaginary minimal steps of normal stress during rapid loading.

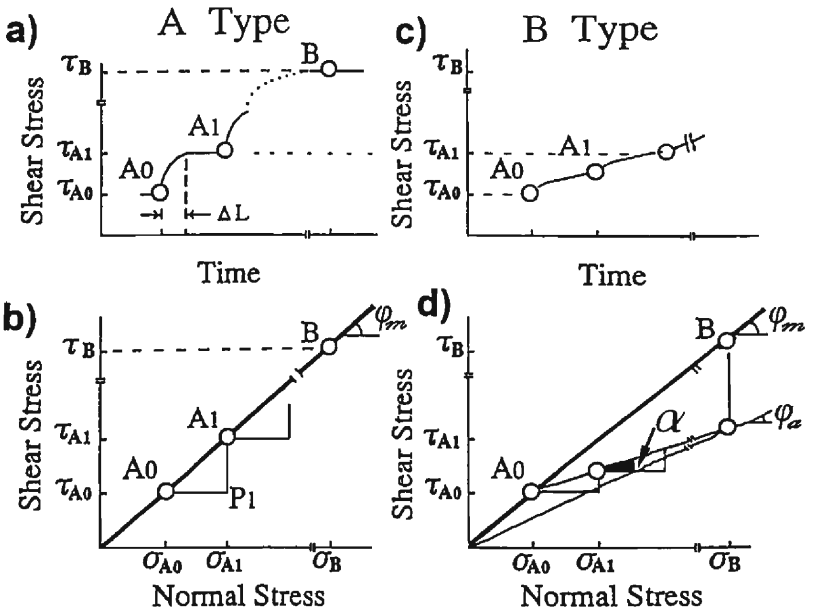

Fig. 7. Possible interpretation of Test A and Test B in **Fig. 5** in the time series change of shear stress (a) and c)) and the stress path (b) and d)).

tion, but the process of deformation to reach the plastic failure state.

3. 3. Comparison of the results of rapid loading tests on dry samples with those on saturated samples

To compare the shear behavior of dry soils and saturated soils during rapid loading, a rapid loading test (Test C) on the same saturated sample was carried out with the same test procedure and at a faster shear speed (10 cm/sec) than that of Test A (1.2 cm/sec) in **Fig. 5**. The test results are presented in **Fig. 8**. When normal stress is increased up to 3.5 kgf/cm^2 for 2 seconds, shear strength did not increase significantly. The stress path of Test C (saturated sample) are similar with that of Test B (dry sample) in **Fig. 5** at first glance. The deviation of stress path in Test C from the failure line should not be due to the state shift from the plastic failure state to the pre-failure deformation state, because of much higher shear speed.

In **Fig. 9**, the changes in shear resistance after rapid loading are presented for dry sample (Test B), and saturated sample (Test C). For dry sample, shear resistance increases linearly after loading and soon reaches shear strength at failure. This point corresponds to the shear displacement of 3 cm. This shear displacement is necessary for the sample to return to the plastic failure state. For saturated sample, shear resistance reaches shear strength at failure when the shear displacement reaches 20 m. The length of time required for shearing over 20 m is necessary for the generated excess pore pressure to fully dissipate.

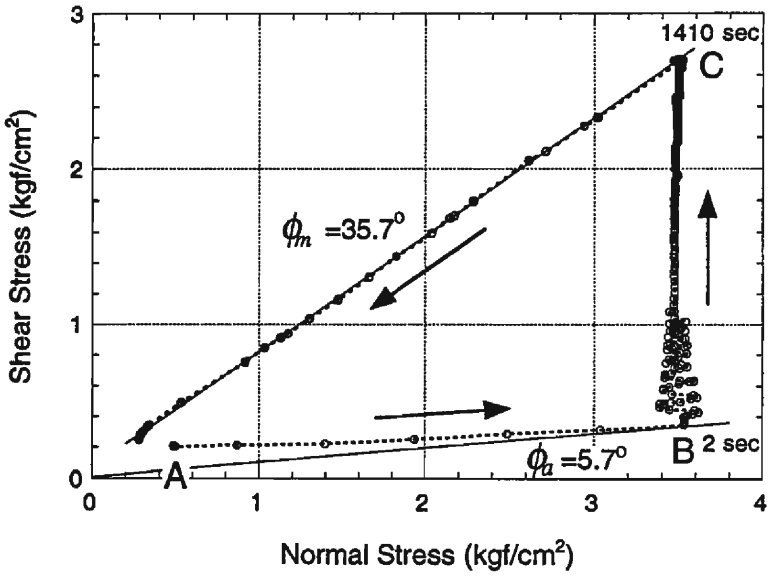

Fig. 8. Rapid loading ring shear test (Test C) of saturated sample from the Kyoto University campus (V_S/V_L =10.0).

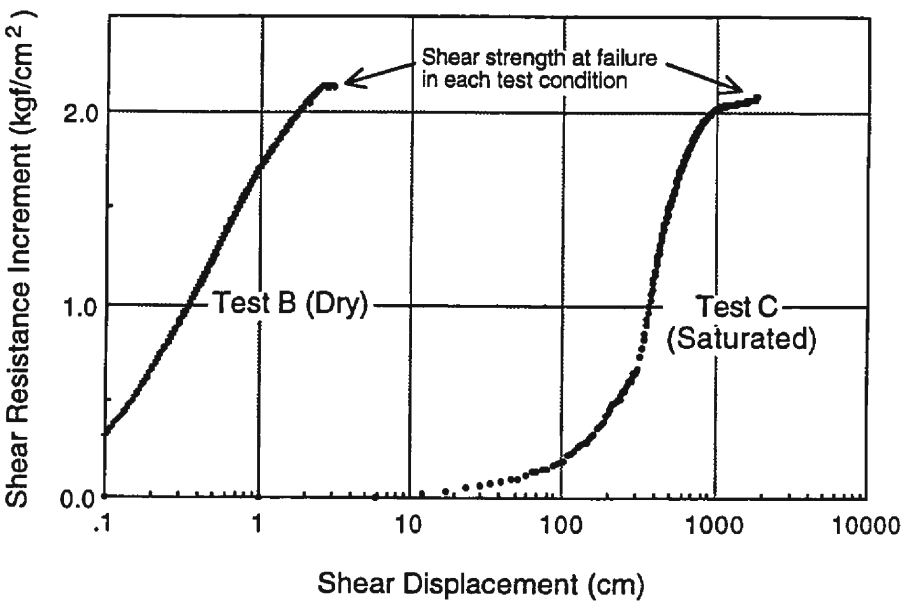

Fig. 9. Difference in shear resistance increment after rapid loading for dry sample (Test B) and the saturated sample (Test C).

3. 4. Critical ratio between shear speed and loading speed to keep the plastic failure state during rapid loading

In real landslides, the state of sliding surface during motion must always be in the plastic failure state. Therefore, the test to reproduce the rapid loading state of long run-out landslides in the ring shear apparatus should be done under the condition where in the plastic failure state during rapid loading is maintained. It is basically important to study the mechanism of shear resistance mobilized during rapid loading in dry soils. Thus, a series of tests for the same dry soil sample from Kyoto University campus were conducted to obtain the critical shear speed/loading speed ratio to keep the plastic failure state.

The test procedure is the same as illustrated in **Fig. 7-a**). A certain normal stress is loaded, then shear rotation is given until the shear stress reaches a constant value, i.e, the failure line, and shearing is stopped. As the next step, an increment of normal stress is supplied, and shear rotation is continued until the plastic failure state is recovered. The same procedure was repeated at various steps of normal stress. The increments of normal stress used ($\Delta\sigma$) were 0.25, 0.5, 0.75, and 1.0 kgf/cm^2. Shear displacement (Δl) during shear rotation is measured. From the results of those tests, the relationship between the shear displacement divided by loaded normal stress ($\Delta l/\Delta\sigma$) and the change of shear resistance divided by loaded normal stress ($\Delta\tau/\Delta\sigma$) are plotted by dotted lines in **Fig. 10**. Over the above mentioned range of $\Delta\sigma$, most of the plots are located along a common curve. Shear resistance divided by loaded normal stress ($\Delta\tau/\Delta\sigma$) increases in a concave manner, and converges to the tangent of a friction angle (ϕ_m) which is

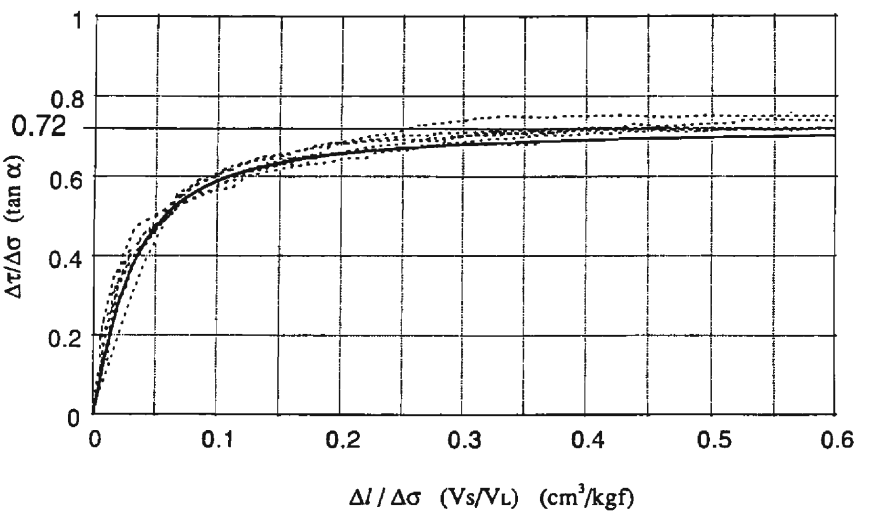

Fig. 10. Relationship between the change of shear strength divided by loaded normal stress and the shear displacement divided by loaded normal stress of the sample from the Kyoto University campus. Dotted lines: Experiments, Solid line: Calculated by Equation (1).

0.72 ± 0.01.

The ordinate of this figure ($\Delta\tau/\Delta\sigma$) is equivalent to $\tan\alpha$, where α is shown in **Fig. 7-d**). The value of tana is between 0 and $\tan\phi_m$.

In order to obtain the function to express the curve of the test results in **Fig. 10**, the following relationship between ($\Delta l/\Delta\sigma$) and ($\Delta\tau/\Delta\sigma$) may be presumed:

$$\Delta\tau/\Delta\sigma=\tan\phi_m \cdot \left\{1-\frac{b}{(\Delta l/\Delta\sigma)^a+b}\right\} \tag{1}$$

Constants were obtained by the method of least square fitting as: $a=1.2$ and $b=0.013$ for the sample.

Let us consider the condition in which the plastic state is always kept during rapid loading.

The abscissa ($\Delta l/\Delta\sigma$) of **Fig. 10** is equivalent to the ratio of shear speed (V_S) to loading speed (V_L).

Let $x=V_S/V_L$, and define $f(x)$ as

$$f(x)=\left(1-\frac{b}{x^a+b}\right) \tag{2}$$

$f(x)$ is the ratio of $\tan\alpha$ and $\tan\phi_m$. The plastic failure state is assumed to be kept within an error of 1.0 %, provided that $\frac{\tan\alpha}{\tan\phi_m}\leq 0.99$. At the critical condition, $f(x)=\frac{\tan\alpha}{\tan\phi_m}=0.99$, and $x=1.25\ \mathrm{cm^3/kgf}$ is obtained from Equation (2). Therefore, the critical test condition for plastic failure state is given by

$$V_S=1.25 \cdot V_L \tag{3}$$

where V_S: shear speed (cm/sec), V_L: loading speed ($\mathrm{kgf/cm^2/sec}$).

Many rapid loading tests on the soil sample from Kyoto University campus were conducted at various shear and loading speeds. Tests in which those stress paths were regarded to be the same as Type A in **Fig. 5** (straight line along the failure line) are plotted as circles in **Fig. 11**; tests in which those stress paths are regarded to be similar to Type B in **Fig. 5** are plotted as crosses. The critical condition given by Equation (3) is drawn as a solid line in the figure. The line divides well into two groups. The conditions for Test A, Test B and Test C are also revealed. Test A and Test C are over the critical line, and Test B is below the line. Plot S is the test condition of the saturated sample taken from the Sale landslide in **Fig. 13**.

4. Measurement of the Apparent Friction Angle and the Pore Pressure during Undrained Loading

4. 1. Variation of the friction angle due to normal stress loading under undrained condition

In 1983, a landslide took place at Mt. Sale in China. It slipped down on alluvial deposits for 1 km with high mobility (average velocity = 13–14 m/sec).

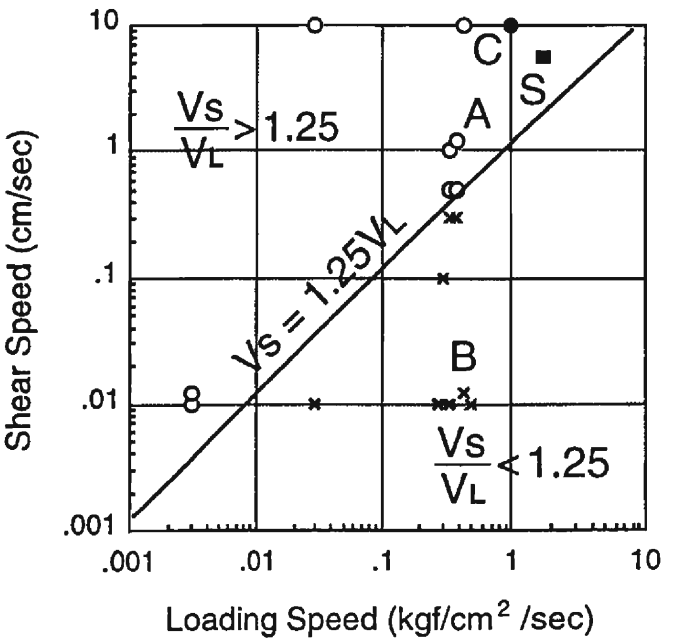

Fig. 11. Relationship between loading speed and shear speed during rapid loading test of dry samples from the Kyoto University campus. Circles represent the type of stress path in Test A, while crosses represent the type of stress path in Test B. Test condition of Test A, Test B and Test C are marked as Point A, Point B and Point C.

There was no rainfall or earthquake at that time, and 220 people were killed. **Fig. 12** is the central section of the Sale landslide which was re-drawn from a geological map prepared by the Gansu Geological Bureau (1986), and the sampling point is illustrated in **Fig. 12**.

The landslide mass traveled over almost the entire length of the flat alluvial deposit up to the main river probably because of the undrained loading on the saturated alluvial deposit. To verify this idea, undrained loading test was carried out using the sample collected from the alluvial deposit of the Sale landslide. Test results are shown in **Fig. 13**.

As for the test procedure, a sample from the alluvial deposits of the Sale landslide was first mixed with water. This slurry was loaded into the shear box, and consolidated under the normal stress of 0.43 kgf/cm^2 corresponding to the location of the sliding surface of 2.0–2.5 m to reproduce the real situation. Pore pressure parameter B_D (ratio of pore pressure increment to loaded normal stress) was measured to be 0.97. Shear was applied slowly in the drained state at the rate of 0.014 cm/sec, and the shear strength before undrained loading was determined (Point A in **Fig. 13-a**)). After switching the valve for drained/undrained condition to the undrained state, the normal stress was increased to 3.73 kgf/cm^2 (Point B) and the pore pressure was measured during shear under the undrained condition. Point

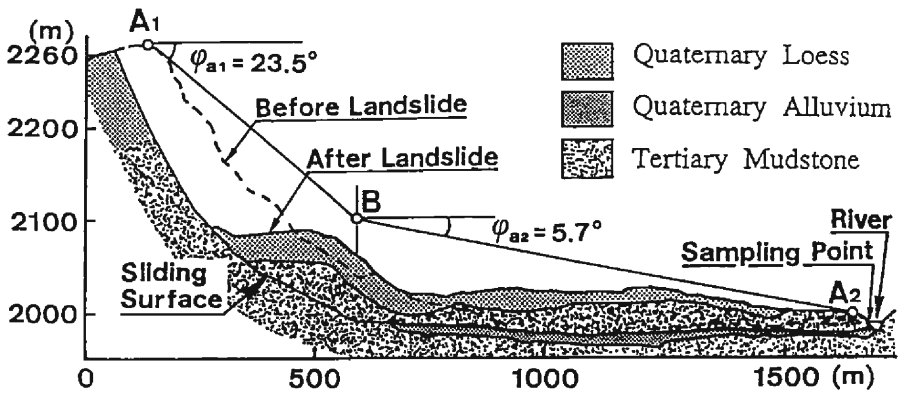

Fig. 12. Section of the 1983 Sale landslide, China (from the geological map by the Gansu Geological Bureau, Sassa and Lee, 1993)

B' represents the state at which pore pressure (2.84 kgf/cm^2) is subtracted from point B. The apparent friction angle mobilized in the undrained loading and the undrained shear condition was 5.2°.

If excess pore pressure is not generated after loading, the stress path will follow the failure line and reach Point C. Because of the generation of excess pore pressure, however, shear stress increased by the amount corresponding to the increment of effective stress and moved to the position much below the failure line (Point B in **Fig. 13-a**)).

To determine the friction angle at zero pore pressure, the shear box was switched to the drained state, and shear was applied slowly at the rate of 0.014 cm/sec keeping normal stress constant. After 500 minutes, shear strength reached Point C which lies on the failure line. The stress path in this case is B-C (total stress path) or B'-C (effective stress path), the measured pore pressure was subtracted from normal stress. Point B' lies slightly below the failure envelope, and it is probably because of the delay of pore pressure measurement at the pore pressure transducer (**Fig. 3**). From this experiment, it was found that the friction angle during motion is 30.1° and the apparent friction angle soon after undrained loading is 5.2°.

From the fact that effective stress path is very close to the failure line of $\phi_m = 30.1°$, it can be maintained that the pore pressure was quantitatively well measured even for soil with permeability as low as 2.9×10^{-6} cm/sec.

4. 2. Variation of the friction angle due to shearing under undrained condition

For torrent deposits of the Ontake debris avalanche, the same procedure was followed as for the alluvial deposit of the Sale landslide and the Lishan landslide. Test results are shown in **Fig. 14**. A sample of the slurry was consolidated under the low stress condition (0.3 kgf/cm^2), and shear was applied slowly at the rate of 0.014 cm/sec in the drained state. Shear strength before loading was measured (Point A). After switching the valve for drained/undrained condition to the un-

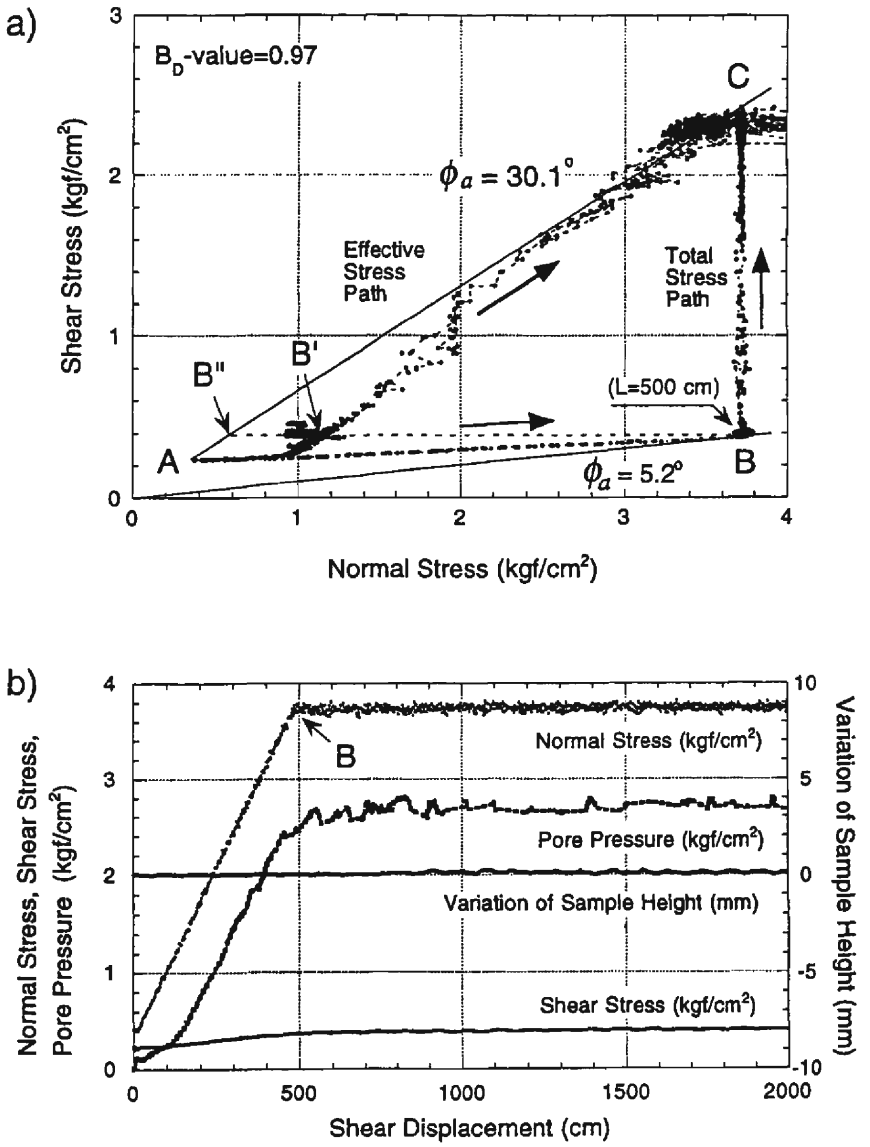

Fig. 13. Undrained loading ring shear test of the saturated alluvial soils from the Sale landslide. a) Stress path, b) Time series data of the normal stress, the shear stress and the pore pressure. A–B (B'): Undrained state, B(B')–C: Drained state, B_D=0.97, e=0.53−0.74.

drained state, shear speed was increased to 12.0 cm/sec. Normal stress was then increased to 2.8 kgf/cm^2 within 3 seconds, and pore pressure was measured at that time (undrained loading and undrained shear condition). Because of the generation of excess pore pressure, shear stress increased by the amount corresponding to the increment of effective stress and moved to a position far from the failure line

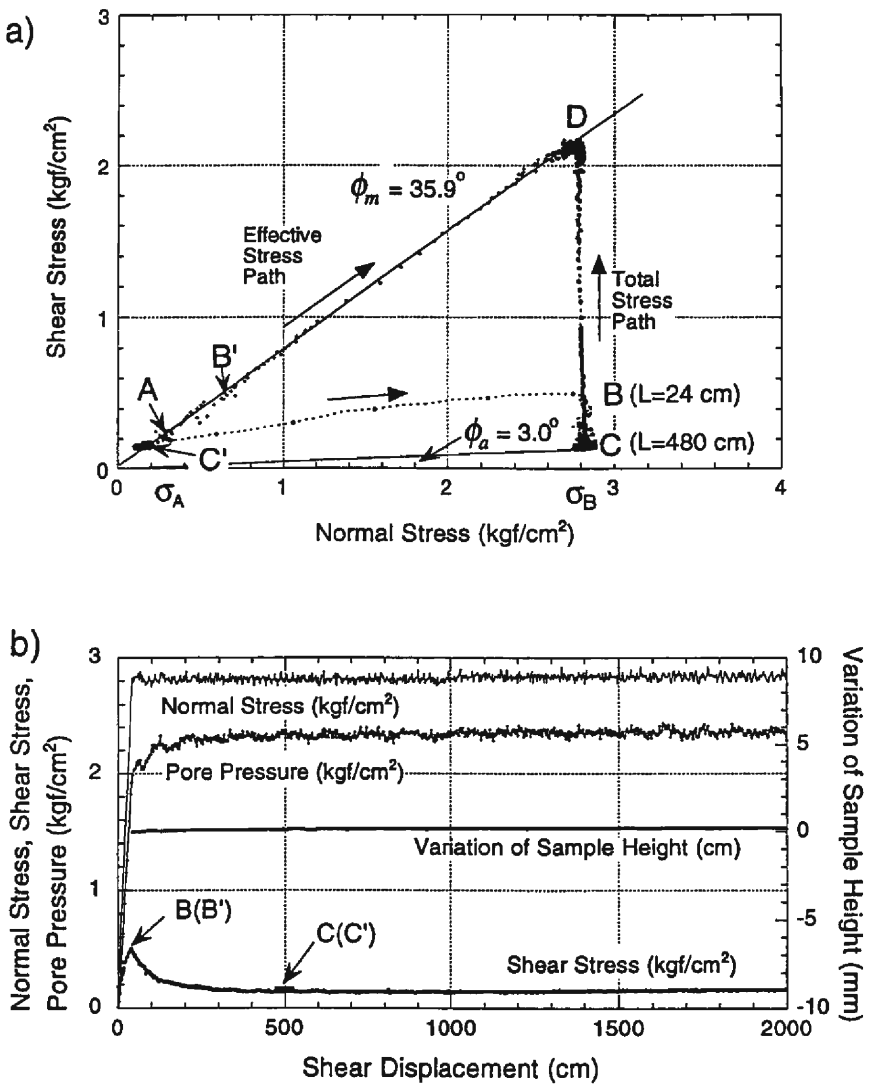

Fig. 14. Undrained loading ring shear test of the saturated sample from the torrent deposits of the Ontake debris avalanche. a) Stress path, b) Time series data of the normal stress, the shear stress and the pore pressure. A–B (B'): Undrained state, B (B')–C: Drained state, B_D=0.93, e=0.50–0.58.

(Point B in **Fig. 14-a**)). Shear was applied continuously at the same shear rate of 12.0 cm/sec keeping normal stress constant. Then, the shear strength decreased down to Point C in 40 seconds after loading (shear displacement corresponded to 480 cm). Point C' represents the effective stress at which measured pore pressure (2.6 kgf/cm^2) was subtracted from Point C. After the shear strength reached Point C, it did not change even under the continuing shear, as shown in **Fig. 14-b**).

After enough stable shear resistance was confirmed, the shear box was switched

to the drained state. With progress of dissipation of pore pressure, shear strength increased gradually and arrived at the failure line in 20 minutes. At that time, pore pressure was almost zero, and the stress path was C-D (total stress path) or C'-D (when pore pressure was subtracted).

In **Fig. 14-a**), the slope angle of the line connecting A-D was 35.9° and a whole stress path was laid on this line. The permeability of this soil is high, so pore pressure was measured without any delay. It is the reason why the effective stress path coincided well with the failure line of 35.9°. The apparent friction angle mobilized under undrained loading condition is 3.0°, and it is very close to 3.4° [(Sassa, 1988a), (Sassa, 1988b)] previously estimated in an indirect way from the pore pressure parameters and the friction angle during motion. In the test of **Fig. 14**, pore pressure parameter ($B_D=0.93$) measured directly before loading was also agreed well with that ($B_D=0.90$) [(Sassa, 1988a), (Sassa, 1988b)] presumed from the relation of the degree of saturation and B-value.

5. Discussion on the Mechanisms of Pore Pressure Generation during Undrained Loading

5. 1. Pore pressure generation due to undrained normal stress loading

Sassa (1988b) presumed that a slip surface becomes close to the direct shear state when the landslide mass moves, and expressed the pore pressure generated in direct shear state as follows;

$$\Delta u = B_D(\Delta\sigma + A_D \cdot \Delta\tau) \tag{4}$$

where Δu : increment of pore pressure, A_D and B_D: pore pressure parameter in direct shear state, $\Delta\sigma$ and $\Delta\tau$: increments of normal stress and shear stress.

Pore pressure parameter B_D means how much the increment of normal stress contributes to the increase of pore pressure, which depends on the degree of saturation and the compressibility of the soil. If soils are not anisotropic, both parameters B_D and B are the same.

Another pore pressure parameter A_D means the increase of pore pressure according to the increment of shear stress when $B_D=1.0$ which means the completely saturated state, and it depends on the volume change according to shearing. It will not be suitable to apply this equation to post-failure behavior because shearing takes places without any shear stress increase in the post failure displacement. However, the concept and the pore pressure parameters A_D and B_D are still convenient to examine the influence of normal stress component and shearing component on the pore pressure generation.

For the saturated sample from torrent deposits of the Ontake debris avalanche, only normal stress was loaded under the undrained condition without any shear displacement. The time series data of the test are shown in **Fig. 15**. A sample of the slurry was consolidated under the normal stress of 0.3 kgf/cm^2. After switching the valve to the undrained state, the normal stress was increased to 2.8 kgf/cm^2

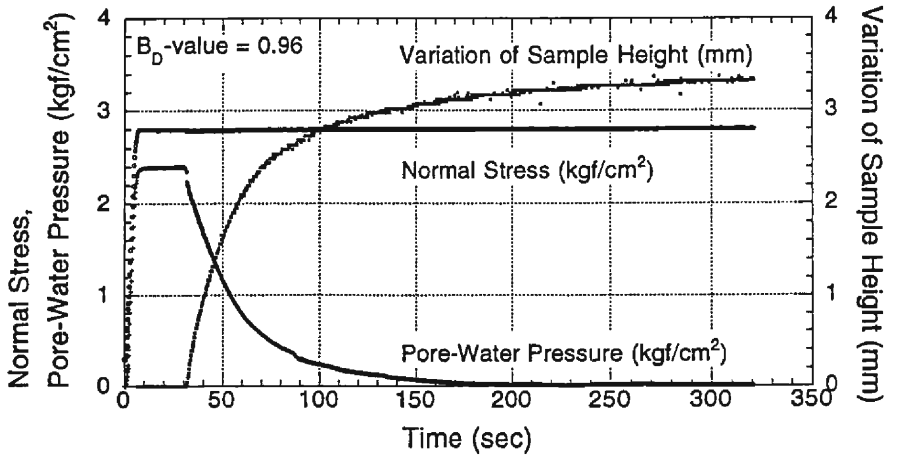

Fig. 15. Undrained normal stress loading test of the saturated sample from the torrent deposits of the Ontake debris avalanche.

within 7 seconds, and the excess pore pressure measured after loading was 2.4 kgf/cm^2. In 30 seconds after undrained loading, the sample box was switched to the drained state. Then, consolidation proceeded with pore pressure dissipation. This pore pressure generation of 2.4 kgf/cm^2 is the same value estimated by Equation (4) because the value of B_D measured after consolidation at the normal stress level of 0.3 kgf/cm^2 by increasing a small amount of normal stress (0.2 kgf/cm^2) was 0.96, the increment of normal stress applied in this test was 2.5 kgf/cm^2 and $0.96 \times 2.5 = 2.4$ kgf/cm^2.

As shown in the stress path of the result of the undrained loading test for the sample from the alluvial deposits of the Sale landslide in **Fig. 13-a**), shear strength did not increase significantly and moved to Point B. It is because the excess pore pressure was generated after loading. The time series data in **Fig. 13-b**) clearly shows that the excess pore pressure was generated according to the increase of normal stress. The increment of normal stress applied under the undrained condition was 3.37 kgf/cm^2, and the excess pore pressure after the loading was measured to be 2.84 kgf/cm^2. Substituting these values and the B_D value measured before the test (0.97) into Equation (4), $(A_D \cdot \Delta\tau)$ becomes-0.44. However, the measured amount of pore pressure is smaller than the real value of generated pore pressure because of the delay of pore pressure transfer. As shown in **Fig. 13-a**), the effective stress path is below the failure line. The delayed measurement of pore pressure is clearly seen in **Fig. 13-b**). Measured pore pressure still continued to increase after Point B at a constant normal stress. If pore pressure were to be correctly measured without delay, Point B' in **Fig. 13-a**) should moved to B" on the failure line. In this case, the generated pore pressure would be 3.17 kgf/cm^2. This value becomes almost the same as the value estimated from $(B_D \cdot \Delta\sigma)$, i.e. $0.97 \times 3.37 = 3.27$ kgf/cm^2. Based

on this test, it can be said for Sale landslide soil that the influence of the second term of Equation (4), namely A_D component, is almost negligible.

5. 2. Pore pressure generation due to undrained shearing and its mechanism

In **Fig. 14**, a considerable amount of pore pressure is generated at a constant normal stress (σ_B) and the shear resistance decreased. It means that a negative dilatancy occurred during shear at a high normal stress level. In order to investigate the effect of pore pressure generation due to undrained shearing without normal stress loading, the test shown in **Fig. 16** was implemented: the sample from the Ontake torrent deposits was firstly consolidated at a normal stress of 2.0 kgf/cm^2, secondly the shear strength was measured in the drained state (Point A). Then, undrained shearing was applied at the speed of 0.1 cm/sec. Pore pressure was significantly generated and the effective stress path moved from Point A to Point B'. Finally, at Point B (B'), pore pressure was no longer generated.

After arriving at Point B, normal stress was raised to 2.8 kgf/cm^2 for 285 minutes with shearing at a constant speed of 0.1 cm/sec. The corresponding stress path was the one between B–C (C'). The pore pressure increase due to the increase of normal stress from Point B to Point C is 0.74 kgf/cm^2, and the corresponding B_D value was 0.93. This was very close to the pore pressure parameter of 0.94, which was measured just after consolidation at σ_B. When shearing is applied continuously after reaching Point C, shear displacement was raised by an additional 1,600 cm (see **Fig. 16–b**)), but the shear resistance did not decrease, which is different from the stress path of B–C in **Fig. 14**. Hence, it is said that a large negative dilatancy took place due to shearing as shown in the stress path from A to B or B' of **Fig. 16**. However, such negative dilatancy did not take place due to shearing after Point C as seen in **Fig. 16–b**).

5. 3. Examination of drainage effects in rapid loading tests

Rapid loading in real landslides is not always same with undrained loading. It is not easy to reproduce similar conditions of drainage under rapid loading in situ by the ring shear test because the height of the shear box is only 6–8 cm, resulting in a much shorter drainage path compared to that in real landslides. However, as one investigation to obtain an index of drainage effects, a rapid loading ring shear test was implemented under the drained setting of the sample box for the alluvial deposits taken from the Sale landslide. The results are given in **Fig. 17**. As for the test, a slurry of the sample was prepared and was first set in the sample box of the apparatus. As the location of the sliding surface was estimated to be 2–2.5 m depth under the ground (Sassa and Lee, 1993), normal stress of 0.38 kgf/cm^2 was applied. Shearing was applied slowly at the rate of 0.014 cm/sec after consolidation, and the shear strength before loading was determined (Point A in **Fig. 17**) in the drained state. Then, in order to simulate rapid loading and rapid shearing, shearing was rapidly applied at the rate of 6.2 cm/sec and the normal stress was rapidly loaded up to 3.4 kgf/cm^2 in 2 seconds. This rapid shearing and rapid normal stress loading

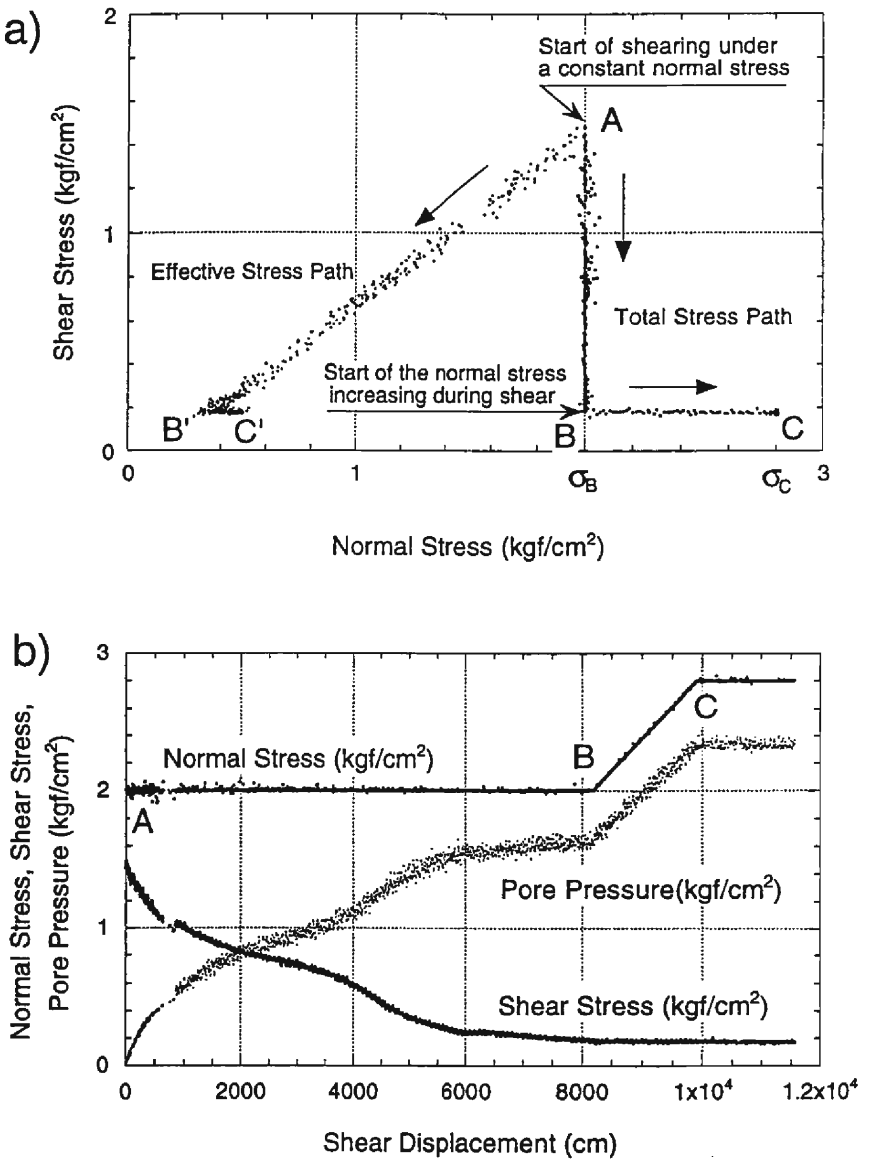

Fig. 16. Uandrained loading ring shear test of the saturated sample from the torrent deposits of the Ontake debris avalanche. a) Stress path, b) Time series data of the normal stress, the shear stress and the pore pressure. $B_D=0.94$, $e=0.76$, Shear speed$=0.1$ cm/sec.

was carried out keeping the shear box always in the drained state. So drainage from the sample was possible through porous metals at both ends of the shear box (illustrated in **Fig. 3**). The test condition maintained is always to keep the soils in the plastic failure state (marked in **Fig. 11** as Point S). Because of the generation of ex-

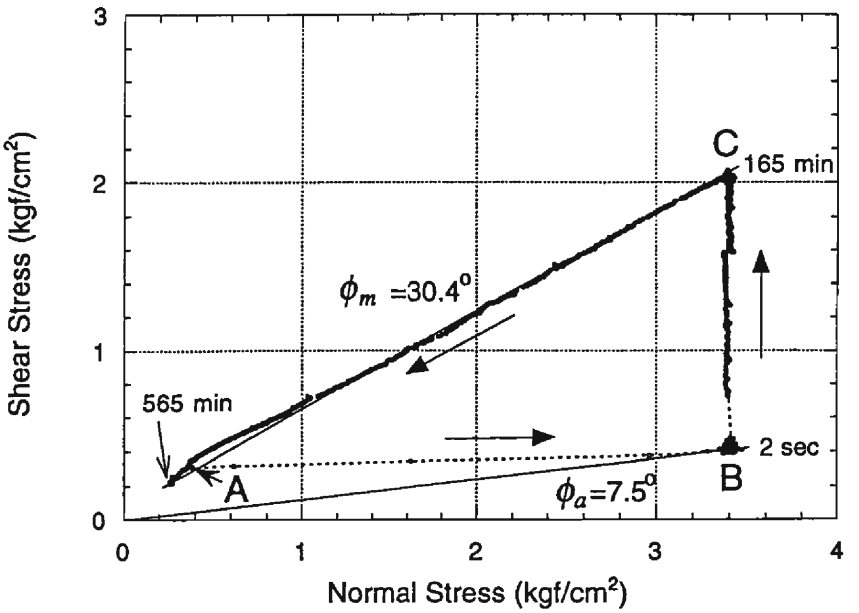

Fig. 17. Rapid loading ring shear test on the saturated alluvial deposits from the Sale landslide (e=0.49−0.64).

cess pore pressure, the stress path deviated from the failure line and moved to the position below the failure line (Point B in **Fig. 17**). After normal stress loading, shear rotation was continued slowly at the rate of 0.014 cm/sec keeping normal stress constant in the drained condition. During this process, excess pore pressure was dissipated slowly and shear resistance increased up to Point C in 165 minutes. Excess pore pressure at this time was considered to be almost zero. Finally, normal stress was decreased to the initial stress keeping the shear rate of 0.014 cm/sec constant. This process was conducted very slowly so as not to generate negative pore pressure.

From the experiment, it was found that the friction angle during motion is 30.4° and the apparent friction angle, which is the slope of the straight line connecting the origin and Point B, is 7.5°. This apparent friction angle is a little higher than 5.2°, the value obtained in the undrained loading test of **Fig. 13** using the same soil from the alluvial deposits of the Sale landslide. After rapid loading, the generated excess pore pressure should be dissipated in the state of one-dimensional consolidation from both ends through the porous metals. The consolidation process was compared to that of Terzaghi's one dimensional consolidation Equation (5).

$$\frac{\partial^2 u_e}{\partial Z^2}=\frac{\partial u_e}{\partial T} \tag{5}$$

where, $Z=z/H$, $T=\frac{c_v t}{H^2}$, z : distance from both end of the sample in the shear box, H : one-half of the sample height, T : time factor, c_v : coefficient of consolida-

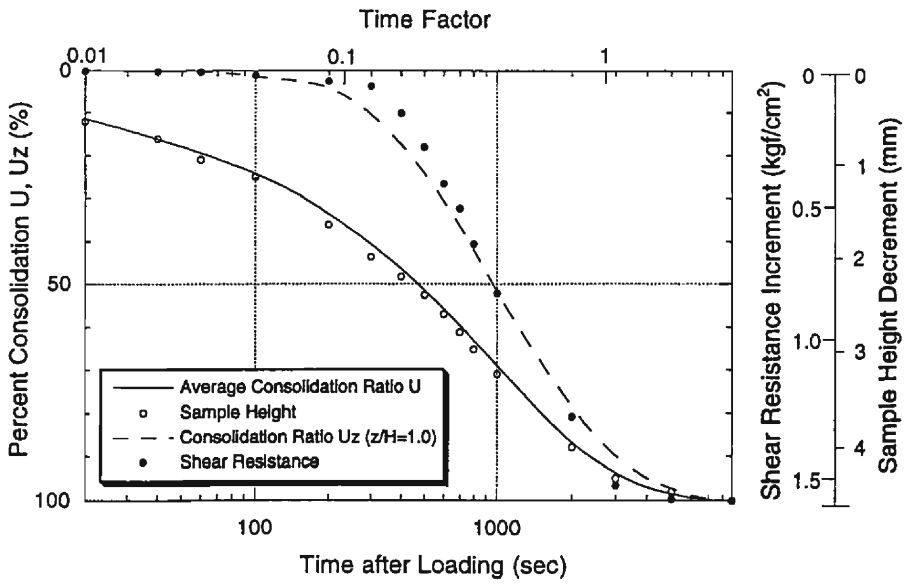

Fig. 18. Shear resistance increment and sample height decrement after rapid loading in comparison with the one-dimensional theory.

tion, u_e : excess pore pressure

In **Fig. 18**, the solid line represents the theoretical relationship between the average consolidation (U) and the time factor by one-dimensional consolidation theory, and the dotted line represents the theoretical degree of consolidation at the center of sample (Uz, $z/H=1.0$); at the shear plane in this case. The change in sample height decrement after rapid loading (B–C in **Fig. 17**) is represented by unfilled circles, which correspond to the change of the average consolidation. The experimental data fit the theoretical curve (solid curve) very well. The consolidation at the center of the sample corresponded to the degree of dissipation of pore pressure at the center of the sample (shear surface in this case), which means the increase in shear resistance along the shear plane by $(-\Delta u \cdot \tan\phi_m)$. The increase in shear resistance during the process of consolidation is represented by filled circles. Those plots are also almost near the theoretical curve (dotted curve). Thus, the change in shear resistance after rapid loading (B–C) is regarded as the process of dissipation of pore pressure in the state of one-dimensional consolidation. The consolidation at the center of the sample (shear plane), namely the increment of shear resistance is almost zero during the first 50 seconds after rapid loading as shown by the filled circles. Though the thickness of the sample is as thin as 6 cm and the pore pressure can be dissipated from both the upper and lower faces of the sample, the undrained condition is kept at the center of the sample during and after rapid loading for 50 seconds or so because the permeability is as low as 2.9×10^{-6} cm/sec. Therefore,

the apparent friction angle of 7.5° obtained from **Fig. 17** is not far from the one (5.2°) obtained under the undrained condition. This finding suggests that undrained loading is very probable in the natural situation.

6. Conclusion

(1) The behavior and the mechanism of shear resistance during rapid loading for dry sample were investigated. When a certain increment of normal stress is given, a certain amount of shear displacement is necessary for shear strength to reach the failure line, i.e. the state of plastic failure. Therefore, when the shear speed to give a necessary shear displacement was not great enough compared to the loading speed to give an increment of normal stress in time, the stress path deviates from the failure line even if the stress was on the failure line before rapid loading. It was found that there are two cases in which the stress path deviates from the failure line by rapid loading, 1) The soil state becomes that of pre-failure deformation due to insufficient shear speed compared to the given loading speed, 2) Excess pore pressure is generated due to rapid loading in the soils, whereby the total stress path deviates from the failure line though the effective stress path remains on the failure line. The critical relationship between shear speed and loading speed wherein the plastic failure state during rapid loading was maintained was deduced (**Fig. 11**).

(2) The high-speed high-stress ring shear apparatus was improved so that the undrained tests were possible and pore pressure generated in the soils could be measured during a large shear displacement. Using this modified apparatus, undrained loading ring shear tests were carried out for saturated samples taken from the alluvial deposits of the 1983 Sale landslide in China and the torrent deposits of the 1984 Ontake debris avalanche in Japan. In these tests the generation of pore pressure during undrained loading was exactly monitored, giving an experimental and quantitative verification by real measurement of pore pressure and direct measurement of the apparent friction angle to the hypothesis proposed by Sassa *et al.* (1989, 1992) and Sassa (1992) that undrained loading phenomenon associated with the motion of landslide must cause the generation of pore pressure producing a low coefficient of friction.

(3) The mechanism of pore pressure generation during undrained loading on saturated soils was investigated. 1) In the stress path during the undrained loading test for fine silty grain sample from the alluvial deposits of the Sale landslide, the generated pore pressure and the value estimated from ($B_D \cdot \Delta\sigma$) were almost same. This means that most of the excess pore pressure in the undrained state was generated by normal stress loading (**Fig. 13**). 2) In the results of the undrained shearing tests for coarse volcanic grains from the torrent deposits of the Ontake debris avalanche, considerable excess pore pressure was generated under constant normal stress loading and the apparent friction mobilized during motion was very small (**Fig. 14** and **Fig. 16**). This pore pressure generation

suggests the negative dilatancy caused by grain-crushing due to shearing under an increase in normal stress. Hence, it was found that the low apparent friction angle mobilized during the motion of landslides was caused by the excess pore pressure generated from the volumetric decrease due to grain-crushing during shear and also from the consolidation due to normal stress loading.

Acknowledgements

This paper was submitted by Jong-hak Lee for the degree of doctor of science, Kyoto University.

Research Associate Hiroshi Fukuoka and postgraduate students of the Landslide Section, Disaster Prevention Research Institute, Kyoto University are acknowledged for their cooperation throughout this study.

Thanks are due to the Professor Yoshimasa Kobayashi, Aso Volcanological Laboratory, Faculty of Science, Kyoto University, and the Professor Kazuo Okunishi, Disaster Prevention Research Institute, Kyoto University for their helpful advice.

References

Bagnold, R. A. (1954): Experiments on a Gravity-Free Dispersion of Large Solid Spheres in a Newton Fluid under Shear, Proc. R. Soc. Lond., Ser. A, 225: 49-63.

Cruden, D. M. and Hungr, O. (1986): The Debris of the Frank Slide and Theories of Rockslide-Avalanche Mobility, Can. Jour. Earth Science, Vol. 23, pp. 425-432.

Davies, T. R. H. (1982): Spreading of Rock Avalanche Debris by Mechanical Fluidization, Rock Mechanics, 15: 9-24.

Fukuoka, H., K. Sassa, C. Vibert and M. Shima (1989): Soil characteristics of the Jizukiyama landslide and the Ontake debris avalanche by the high-speed high-stress ring shear apparatus, Annals, Disas. Prev. Res. Inst., Kyoto Univ., No. 32 B-1, pp. 183-195 (in Japanese).

Fukuoka, H. (1991): Variation of the Friction Angle of Granular Materials in the High-Speed High-Stress Ring Shear Apparatus, -Influence of Re-orientation, Alignment and Crushing of Grains during Shear-, Bull., Disas. Prev. Res. Inst., Kyoto Univ., Vol. 41, Part 4, pp. 243-279.

Gansu Geological Bureau (1986): Geological maps on the Sale landslide.

Gogule, J. (1978): Scale-Dependent Rockslide Mechanisms, with Emphasis on the Role of Pore Fluid Vaporization, In: Rockslides and Avalanches, 1 (Voight, B., ed.) Dev. Geotech. Eng. 14A, pp. 693-705, Amsterdam, Oxford, New York: Elsevier.

Hsü, K. J. (1975): Catastrophic Debris Streams (Sturz-stroms) Generated by Rockfalls, Bull. of Geological Society of America, Vol. 86, pp. 129-140.

Hutchinson, J. N. (1986): A Sliding-Consolidation Model for Flow Slides, Can. Geotech. Jour., Vol. 23, pp. 115-126.

Kobayashi, Y. (1994): Effect of Basal Guided Waves on Landslides, Pageoph, Vol. 142, No. 2, pp. 329-346.

Körner, H. J. (1980): Model Conceptions for the Rock Slide and Avalanche Movement, Proc. Int'l Symp. "INTERPRAEVENT 1980", Vol. 2, 15-55 (in German).

Körner, H. J. (1982): Japanese Translation of Selected Papers form Proc. Int'l Symp. "INTERPRAEVENT 1980", The Erosion Control Engineering (Sabo) Society, Japan.

McSaveney, M. J. (1978): Sherman Glacier Rock Avalanche, Alaska, U. S. A., In: Rockslides and Avalanches, 1 (Voight, B., ed.) Dev. Geotech. Eng. 14A, pp. 197-258, Amsterdam, Oxford, New York: Elsevier.

Melosh, H. J. (1979): Acoustic Fluidization: A New Geologic Process ?, Jour. Geophys. Res., Vol. 84, No. B13, pp. 7513-7520.

Sassa, K. (1988a): Geotechnical Model for the Motion of Landslides, Report of Grant-in-Aid for Scientific Research by Japanese Min. of Education, Science and Culture (No. 61480062), 52 pages.

Sassa, K. (1988b): Special Lecture: Geotechnical model of the motion of landslides. Proc. 5th International Symposium on Landslides, Vol. 1, "Landslides", Editor, Bonnard, A. A. Balkema, pp. 37-55.

Sassa, K., H. Fukuoka and C. Vibert (1989). A New High-Speed High-Stress Ring Shear Apparatus and the Undrained Shear Strength during Motion. Proc. The Japan-China Symposium on Landslides and Debris Flows, pp. 93-97.

Sassa, K. (1992): Landslide Volume-Apparent Friction Relationship in the Case of Rapid Loading on Alluvial Deposits, Landslide News, Japan Landslide Society, No. 6, pp. 16-19.

Sassa, K., H. Fukuoka, J. H. Lee and D. Zhang (1992): Measurement of the apparent friction angle during rapid loading by the high-speed high-stress ring shear apparatus - Interpretation of the relationship between landslide volume and the apparent friction during motion, Proc. 6th International Symposium on Landslides, "Landslides", Bell (ed.), Balkema, Vol. 1, pp. 545-552.

Sassa, K. and J. H. Lee (1993): Measurement of the Apparent Friction Angle During Motion by the High-Speed Ring Shear Apparatus, Journal of Japan Landslide society, Vol. 30, No. 1, pp. 1-10 (in Japanese).

Sassa, K. (1994) : Development of a new cyclic loading ring shear apparatus to study earthquake-induced-landslides. Report for Grant-in-Aid for Developmental Scientific Research by the Ministry of Education, Science and Culture, Japan (Project No. 03556021), 106 pages.

Scheidegger, A. E. (1973): On the Prediction of the Reach and Velocity of Catastrophic Landslides, Rock Mechanics, 5: 231-236.

Shoaei, Z. and K. Sassa (1994). Basic Study on the Shear Behavior of Landslides during Earthquake -Excess Pore Pressure Generation in the Undrained Cyclic Loading Ring Shear Tests-. Bulletin of the Disaster Prevention Research Institute, Kyoto University, Vol. 44, pp. 1-43.

Shreve, R. L. (1966): Sherman Landslide, Alaska, Science, Vol. 154, 1639-1643.

Shreve, R. L. (1968): The Blackhawk Landslide, Geol. Soc. Amer., Spec. Paper 108, pp. 1-47.